Development of a 3D high-resolution physical anthropomorphic breast phantom

Ann-Katherine Carton a), Predrag Bakic a), Christer Ullberg b), Andrew D.A. Maidment a)
a) University of Pennsylvania, Philadelphia PA, USA
b) XCounter AB, Svärdvägen 11, SE-182 33 Danderyd, Sweden
[Ann-Katherine.Carton|Predrag.Bakic|Andrew.Maidment]@uphs.upenn.edu
Christer.Ullberg@Xcounter.se

ABSTRACT

Analysis of complex imaging tasks requires a phantom that simulates the patient anatomy. We have developed a technique to fabricate 3D physical anthropomorphic breast phantoms for image quality assessment of 2D and 3D breast x-ray imaging systems. The phantom design is based on an existing computer model that can generate breast voxel phantoms of varying size, shape, glandularity, and internal composition. The physical phantom is produced in two steps. First, the computer model of the glandular tissue, skin and Coopers' ligaments is separated into sections. These sections are fabricated by high-resolution rapid prototype printing using a single tissue equivalent material. The adipose tissue regions in the sections are filled using an epoxy-based resin combined with phenolic microspheres. The phantom sections are then stacked. The phantom is provided with an extra section modified to include iodine-enhanced masses. We fabricated a prototype phantom corresponding to a 450 ml breast with 45% dense tissue deformed to represent a 5 cm compressed thickness. The rapid prototype and epoxy based resin phantom materials attenuate x rays similar to 50% glandular tissue and 100% adipose tissue, respectively. The iodinated masses are between 4.0 and 9.6 mm thick and contain 2.5 mg/ml and 5 mg/ml iodine. Digital mammography and digital breast tomosynthesis images of the phantom are qualitatively similar in appearance to clinical images. In summary, a method to fabricate a 3D physical anthropomorphic breast phantom has been developed with known ground truth in the form of a companion voxel phantom. This combined system of physical and computational phantoms allows for both qualitative and quantitative image quality assessment.

Keywords: Anthropomorphic phantom, digital mammography, digital breast tomosynthesis, iodine-enhanced imaging

1. INTRODUCTION

Physical phantoms are essential tools in the characterization and optimization of x-ray imaging systems. In mammography, phantoms typically consist of a homogenous material in which appropriate test objects are embedded. Such phantoms are used to evaluate low- and high-contrast detectability, photo-timer performance, linearity of the detector response, spatial resolution, and noise response.

However, more realistic imaging tasks require an anthropomorphic breast phantom; *i.e.* a tissue equivalent phantom which produces x-ray images similar to those of a real breast. To the best of our knowledge, the only commercially available anthropomorphic breast phantom is "Rachel" (Model 169, Gammex RMI, Madison, WI) [1]. A radiographic projection image of this phantom resembles a mammogram. The application of the Rachel phantom is however limited to the evaluation of a subset of 2D projection imaging systems because this phantom does not simulate the 3D breast anatomy.

In this work, we present a method to fabricate high resolution anthropomorphic breast phantoms simulating fine breast tissue details in 3D. We believe that such phantoms can be used for performance testing of 2D and novel 3D breast x-ray imaging systems. The phantom design is based upon a previously developed computer model that can simulate breast voxel phantoms. Here, material selection and the physical phantom fabrication technique are described. Full field digital mammography (FFDM) images and reconstructed digital breast tomosynthesis (DBT) images of our first prototype phantom are shown. In addition, we have adapted the prototype phantom to include iodine-enhanced lesions. This enhancement to the phantom allows assessment of the performance of contrast-enhanced (CE) FFDM and CE-DBT imaging systems.

Medical Imaging 2010: Physics of Medical Imaging, edited by Ehsan Samei, Norbert J. Pelc,
Proc. of SPIE Vol. 7622, 762206 · © 2010 SPIE · CCC code: 1605-7422/10/$18 · doi: 10.1117/12.845367

2. PHANTOM DESIGN

The phantom design is based upon an existing computer model that can generate breast voxel phantoms of varying composition, size, and shape (Figure 1 a) [2-4]. Briefly, the voxel phantom consists of two large scale regions. The inner region is composed of fibroglandular tissue in which medium scale compartments of adipose tissue are embedded. The outer region is composed of adipose tissue organized into medium scale compartments supported by a matrix representing the Cooper's ligaments. The phantom is covered by a layer of skin. Breast deformation during breast compression in the mammographic or digital breast tomosynthesis (DBT) imaging process is simulated using a finite element model (Figure 1 b) [5].

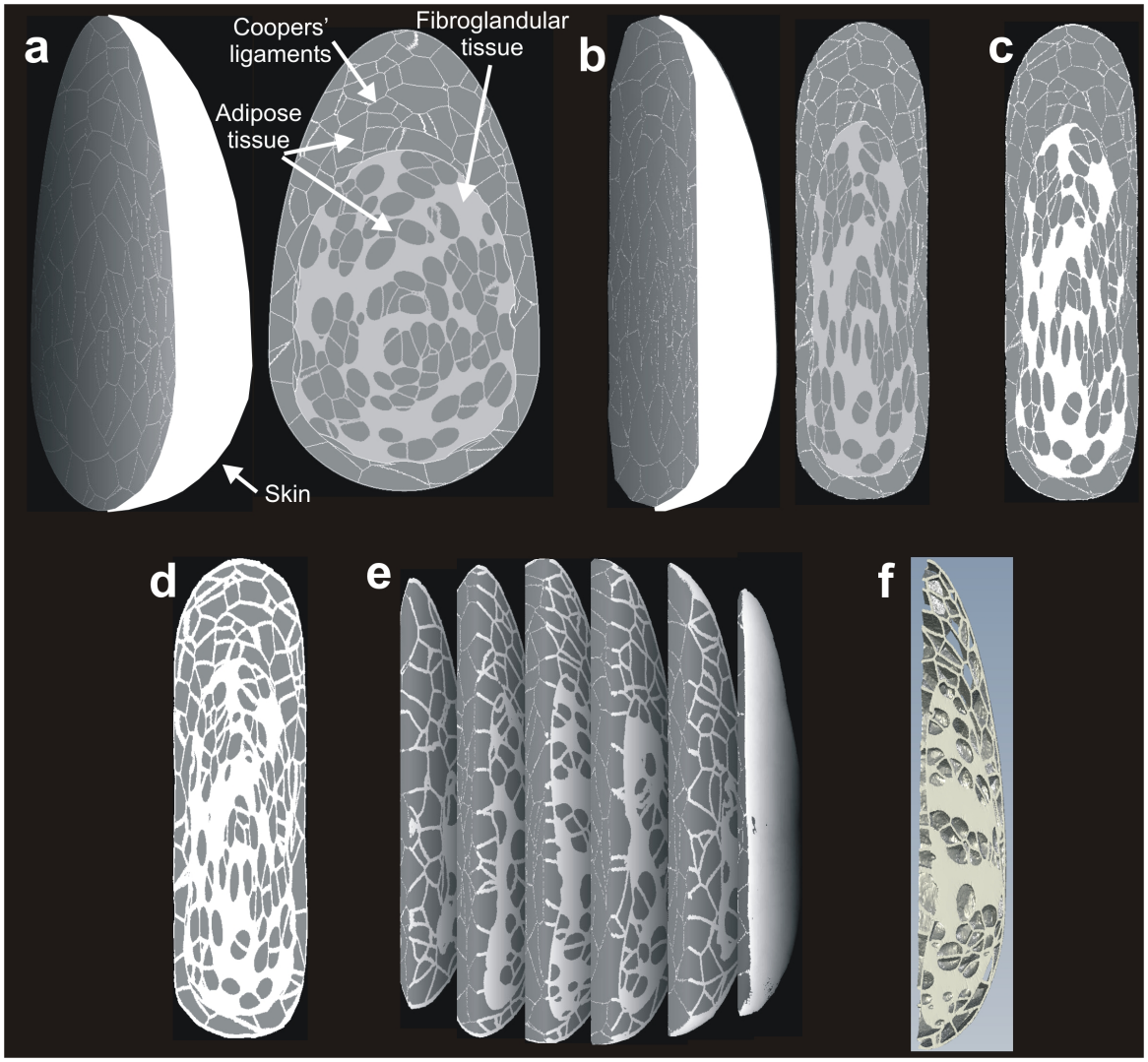

Figure 1: Overview of the phantom design. Outline of the breast voxel phantom and coronal section through the breast voxel phantom before (a) and after (b) simulating breast compression; Coronal section of the voxel phantom divided into two classes determined by the fabrication technique and phantom materials (c); Coronal section of the voxel phantom after applying morphological dilation to the fibroglandular tissue, skin and Cooper's ligaments (d); Portion of the voxel phantom consisting of the fibroglandular tissue, skin and Cooper's ligaments separated into sections (e); Section for rapid prototyping (f).

Prior to phantom fabrication, the following preprocessing steps are performed. The four tissue types in the voxel phantom are divided into two classes determined by the fabrication technique and phantom materials (Figure 1 c). The first class consists of fibroglandular tissue, skin, and Cooper's ligaments; these tissues are fabricated by rapid prototype (RP) printing using a single tissue equivalent material. The second class consists of adipose tissue which is fabricated using an epoxy-based resin ($EBR_{adipose}$) that is manually cast in the compartments of the RP material. Next, morphological dilation with a spherical structural element of radius equal to 3 voxels is applied to the class consisting of fibroglandular tissue, skin, and Cooper's ligaments to ensure that the Cooper's ligaments are continuous and provide structural stability (Figure 1 d). Next, the voxel phantom is separated into sections to expose the adipose tissue compartments in the RP material so they can later be filled with $EBR_{adipose}$ (Figure 1 e). The voxel phantom composed of fibroglandular tissue, skin, and Cooper's ligaments is then converted to a stereolithography (STL) data format required for RP printing (Figure 1 f). We performed the tissue labeling, section slicing, surface modeling, and STL conversion using Mimics software (Materialise NV, Leuven, Belgium).

The breast voxel phantom used to fabricate the prototype physical phantom corresponded to a 450 ml breast deformed to a 5 cm compressed thickness. After applying morphological dilation, the phantom consisted of 45% dense tissue by volume. The breast voxel phantom was then separated into six sections; the four inner sections were 1 cm thick and the two outer sections were 0.5 cm thick. The breast voxel phantom was computed with 200 μm^3 voxel size.

In addition, a duplicate of one of the inner phantom voxel sections was modified to simulate iodine contrast-agent accumulation in lesions. We simulated lesions with the shape of a Limaçon revolved about its longitudinal axis, which is given by the equation $\left(x^2+y^2+z^2-2bx\right)^2=b^2\left(x^2+y^2+z^2\right)$ (Figure 2). The limaçon lesion shape was chosen for two reasons. First, based upon practical considerations, the top surface of a 3D limaçon provides a large enough opening to allow the lesion compartment to be easily filled with an iodinated phantom material. Second, a limaçon has smooth edges resembling real breast lesions. The magnitude of b was varied to obtain lesions with thicknesses between 4.0 mm and 9.6 mm and widths between 4.6 mm and 10.6 mm. In total ten lesions with five different sizes were simulated, two lesions were created of each size (see Table 1). The lesion locations are indicated on the tomographic section shown in Figure 3.

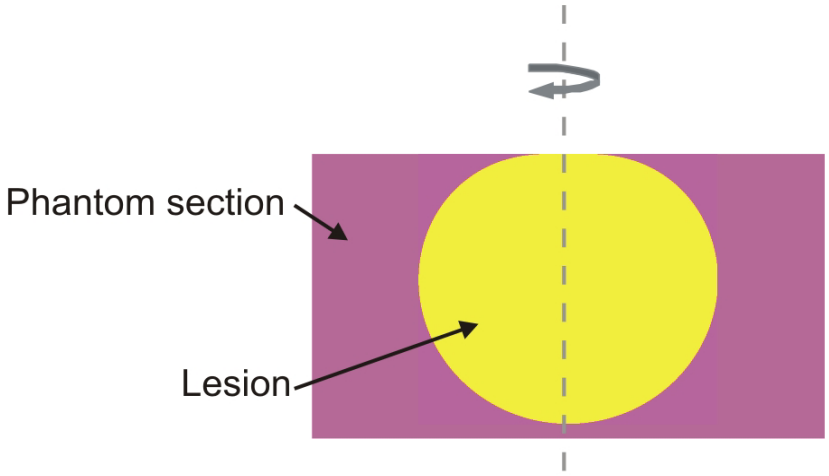

Figure 2: Profile of a simulated lesion embedded in a phantom section. The simulated lesion has the shape of a Limaçon revolved around the indicated axis.

Figure 3: Tomographic section of the segmented breast voxel phantom indicating the lesion positions (dark brown and light orange circles). The brown circles refer to the lesion compartments filled with EBR_{iodine} containing 5.035 mg/I ml, the orange circles refer to the lesion compartments filled with EBR_{iodine} containing 2.575 mg/I ml. The diameters of the circles are proportional to the sizes of the lesions.

Table 1: Lesion characteristics. In total ten lesions were simulated; one of each size and iodine concentration.

Lesion depth [mm]	Lesion width [mm]	Areal density [mg I/cm^2]	
		5.035 mg I/ml	2.575 mg I/ml
9.6	10.6	4.83	2.47
8	8.8	4.03	2.06
6.2	7.0	3.12	1.60
4.8	5.4	2.42	1.24
4	4.6	2.01	1.03

3. MATERIAL SELECTION

FC-720 (Objet Geometries Ltd., Rehovot, Israel), an acrylic based photopolymer, was used to fabricate the voxel phantom sections composed of fibroglandular tissue, skin, and Cooper's ligaments. We selected FC-720 because of its radiographic properties and rigidity; FC-720 has x-ray attenuation properties equivalent to 50% glandular tissue and was the most rigid among the available RP materials we compiled. An EBR with 100% adipose equivalency, $EBR_{adipose}$, was created to fill the adipose tissue compartments in the RP product. The $EBR_{adipose}$ was fabricated using a method similar to that described previously [6]. An iodinated EBR, EBR_{iodine}, was developed to fill the lesion compartments. EBR_{iodine} containing 5.035 mg/I ml and 2.575 mg/I ml were created; these concentrations are considered clinically relevant [7]. The iodinated EBR was fabricated based on the method described by Hill *et al*. [8].

The glandular equivalency of the RP and $EBR_{adipose}$ phantom materials were experimentally assessed from signal intensity (*SI*) measurements in images acquired with a Selenia Dimensions DBT prototype (Hologic Inc., Bedford, MA). These characteristics were assessed using 1 cm-thick RP and $EBR_{adipose}$ phantom samples, and 1 cm-thick tissue equivalent samples with known glandularity (CIRS, Norfolk, VA). The samples were imaged using a W/Rh target/filter x-ray beam at tube voltages from 22 to 32 kV and using a W/Cu target/filter x-ray beam at tube voltages from 40 to 49 kV. *SI* measurements were performed in linear projection images after flat-field and offset corrections were applied by the manufacturer. The glandular equivalency of the phantom materials was measured in terms of the primary attenuation of the phantom materials relative to tissue equivalent materials with known glandularity. The relative attenuation, *R*, was computed as:

$$R(E) = \frac{\overline{SI}_p(E) - \overline{SI}_g(E)}{\overline{SI}_g(E)} \times 100\%$$

where $\overline{SI}_p(E)$ and $\overline{SI}_g(E)$ are the means in the per-pixel signal intensity at tube voltage E in images of the RP or $EBR_{adipose}$ phantom sample, p, and in images of the breast tissue equivalent material, g, with known glandularity. The tissue equivalent materials had glandularities ranging from 0% to 100%. The geometry used to assess $\overline{SI}_p(E)$ and $\overline{SI}_g(E)$ is shown in Figure 4.

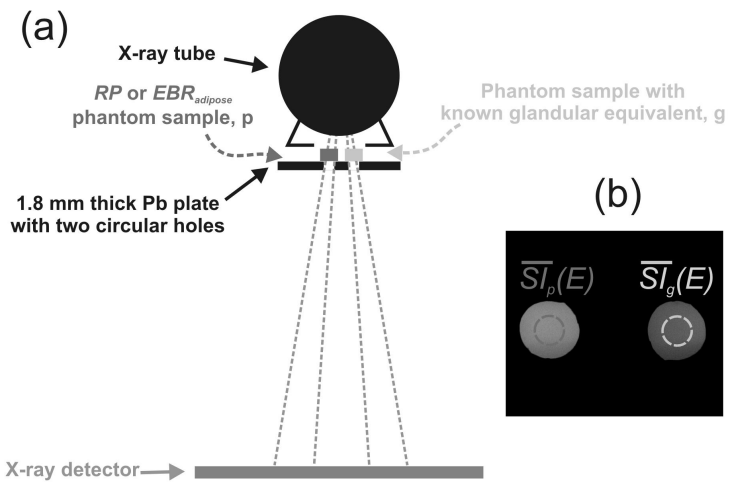

Figure 4: (a) A narrow beam geometry was used to assess *R*, while limiting the influence of scattered radiation. (b) The mean *SI* was computed in 1 cm-diameter circular regions centered in the test regions.

Figure 5 shows the glandular equivalence of the EBR$_{adipose}$ (Figure 5 a) and RP (Figure 5 b) phantom materials as a function of kV. These figures show that the EBR$_{adipose}$ and the RP materials have linear attenuation properties that are very similar to 100% adipose tissue and 50% glandular tissue, respectively, for x-ray beam energies typically applied in mammography. Similar linear attenuation properties were found when using higher energy beams (*i.e.* W/Cu target filter and 40-49 kV) typically applied for iodine contrast-enhanced imaging (not shown).

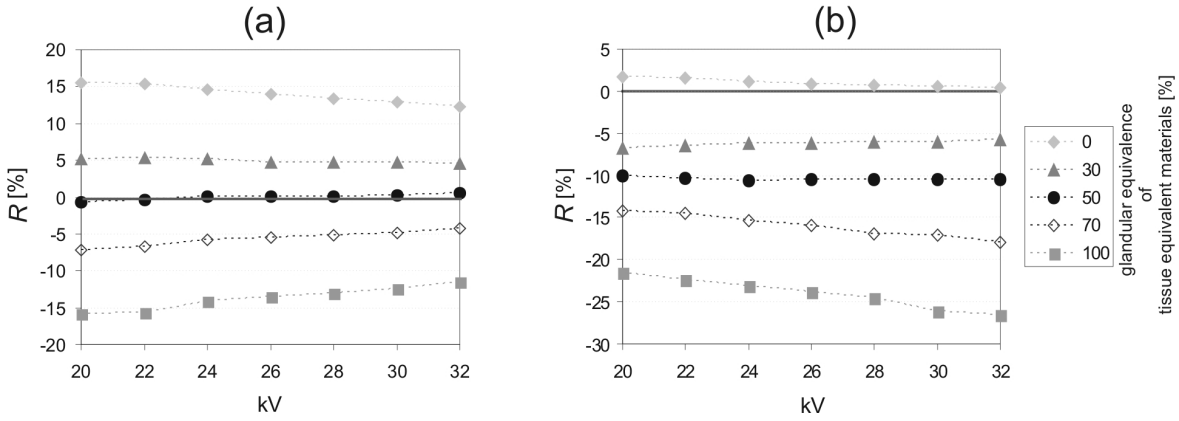

Figure 5: *R* for the RP (a) and the EBR$_{adipose}$ (b) phantom materials as a function of kV using a W/Rh target/filter combination. When *R*=0 (indicated by the red line), the phantom materials have the same glandular equivalence as the tissue equivalent materials with known glandular equivalence.

4. PHANTOM FABRICATION

The phantom sections representing fibroglandular tissue, Cooper's ligaments, and skin, were fabricated using high-resolution (16 μm^3 voxels) RP printing. Next, a thin primer, consisting of a simple EBR, was applied to the surface of the adipose compartments. Then, the adipose tissue compartments were filled with EBR$_{adipose}$. The EBR$_{adipose}$ was poured in thin layers to allow air bubbles to escape from the highly viscous EBR$_{adipose}$. Each layer was left to cure before the next layer was applied. Periodically throughout this process, radiographs of the phantom sections were acquired to localize remaining air bubbles; the largest bubbles (~ 0.5 mm in diameter) were broken with a needle before the next layer was poured. Finally, the phantom sections were sanded to remove excess EBR$_{adipose}$.

The lesion section underwent one addition processing step where the lesions were filled with EBR_{iodine}. Five lesions, one of each size, were filled with EBR_{iodine} containing 5.035 mg I/ml and the other five lesions were filled with EBR_{iodine} containing 2.575 mg I/ml (Figure 3 and Table 1). The phantom section containing the lesions was sanded again to remove excess EBR_{iodine}. Finally, the phantom sections were stacked together. Figure 6 a shows the six phantom sections corresponding to the glandular portion, skin and Coopers' ligaments (left) before filling with $EBR_{adipose}$. Figure b shows the six sections filled with $EBR_{adipose}$.

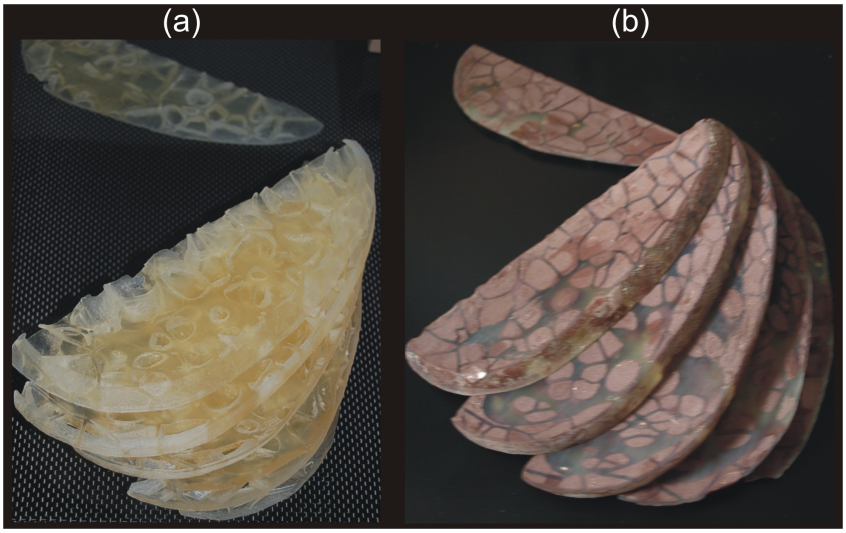

Figure 6: (a) Phantom sections fabricated by rapid prototyping of the fibroglandular portion, skin and Coopers' ligaments and (b) phantom sections after filling with an adipose tissue equivalent $EBR_{adipose}$.

5. PHANTOM IMAGING

Figure 7 shows FFDM and reconstructed DBT images of the prototype physical phantom. The images were acquired with a prototype FFDM/DBT system (Hologic Dimensions, Bedford, MA) using automatic exposure control (AEC). The DBT projection images were reconstructed using a filtered backprojection algorithm. Two MQSA certified mammographers reviewed these images.

The phantoms images were produced with AEC, yielding phototimer parameters that are very similar to those obtained when imaging a real breast with similar thickness and glandular composition. The radiologists reported that the FFDM and DBT images simulate a dense fibroglandular pattern that appears qualitatively similar to that of clinical images and that the grayscale range of adipose and fibroglandular elements approximates the pattern seen in a heterogeneously dense breast, noting that there are still artifacts from air bubbles in the EBR as indicated by the arrows on Figure 7.

Figure 8 illustrates a low-energy (LE), a high-energy (HE), and an iodine-enhanced dual-energy (DE) CE-FFDM image of the phantom containing the section with the iodinated lesions. The images were also acquired with the Hologic Dimensions. The LE image was acquired at 35 kV with a Sn filter in the beam and using a mean glandular dose (MGD) of 0.56 mGy, the HE image was acquired at 49 kV with a Cu filter in the beam and using a MGD of 0.85 mGy. The dose allocation, defined as the proportion of the MGD allocated to the HE image was 0.60. The DE CE-FFDM image was obtained by applying a logarithmic weighted subtraction to the HE and LE images. In this subtraction, a weighting factor was applied that optimally cancels the structured background. Note that the five lesions containing iodine concentrations of 5.035 mg/ml are discernable, while only the three largest lesions containing 2.575 mg/ml iodine concentrations are discernable.

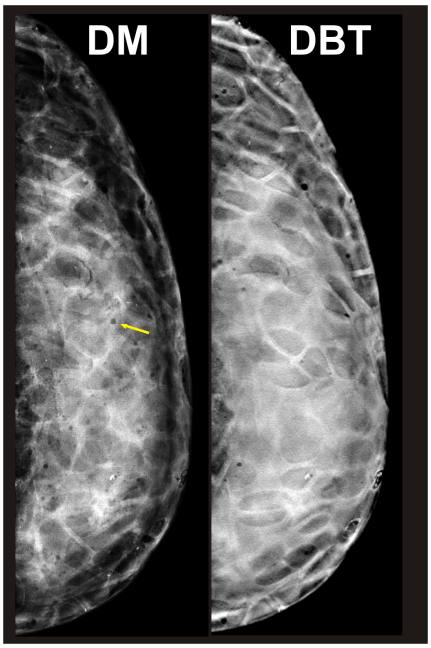

Figure 7: FFDM image (left) and a reconstructed DBT slice (right) of the first prototype physical anthropomorphic phantom. Remaining air bubbles in the $EBR_{adipose}$ are seen as radio-lucent spheres (arrow).

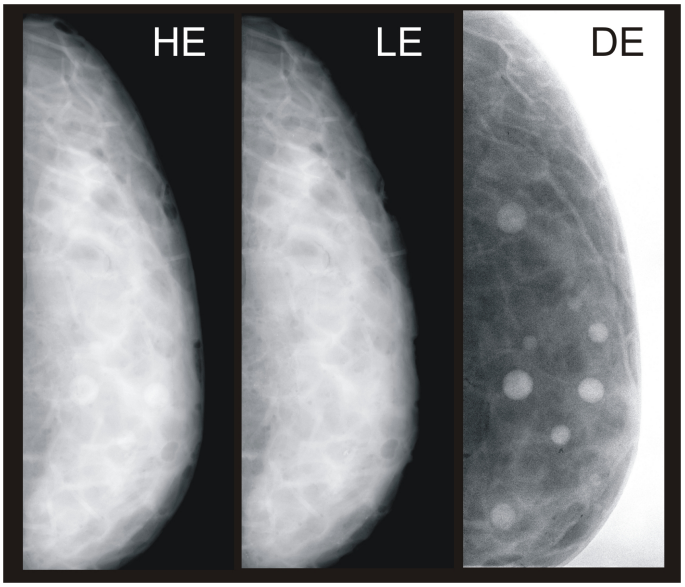

Figure 8: A HE, LE and iodine DE CE-FFDM images of our anthropomorphic physical breast phantom. The HE image was acquired at 49 kV with a Cu filter in the x-ray beam and a MGD of 0.85 mGy. The LE image was acquired at 35 kV with a Sn filter in the x-ray beam and a MGD of 0.56 mGy. The iodine DE-DM image was obtained by applying a logarithmic weighted subtraction. The weighting factor in the subtraction was selected to optimally cancel the background breast tissue.

6. DISCUSSION AND CONCLUSION

The primary attenuation characteristics of the phantom materials selected for the development of the prototype phantom were found to match those of breast tissue at the low x-ray energy range used in mammography and the higher energies used for contrast-enhanced breast x-ray imaging. The agreement of the AEC exposure parameters for the phantom and real breasts with similar composition and compressed thickness indicate that the phantom can be used to assess photo-timer performance. The prototype phantom is provided with an interchangeable section containing iodinated lesions of various concentrations. This makes the phantom valuable as a tool to characterize CE-FFDM and CE-DBT imaging systems. We anticipate that the phantom could be provided with additional sections modified to include micro calcifications, fibers, masses or hollow tumors made externally accessible through tubes.

The current fabrication method is subject to fabrication errors; residual air bubbles are visible on the x-ray images and sanding of the phantom may result in slight differences of thickness. Imperfect background subtraction in the dual-energy CE-FFDM image can be attributed to these defects. The current fabrication method is also very time consuming. Ideally the complete phantom would be fabricated in a single process using rapid prototype printing. This requires that different materials simulating the various tissue types become readily available. Finally, the next phantom version should contain an interlocking system to ensure proper alignment of the sections.

In summary, we have developed a technique for fabricating 3D high-resolution anthropomorphic breast phantoms with known ground truth in the form of a companion voxel phantom. FFDM and DBT images of the first prototype 3D anthropomorphic breast phantom described here have a qualitatively similar appearance to clinical breast images.

ACKNOWLEDGMENT

The physical breast phantom was developed under research grants from XCounter AB (Danderyd, SE) and Hologic Inc. (Bedford, MA). Previous research on the software phantom was funded by NSF Grant IRI-9504363, NIH Grant P01 CA85484, NIH Grant R01 CA102758, and Susan G. Komen Breast Cancer Foundation Research Grant BCTR133506. The contents of this paper are solely the responsibility of the authors and do not necessarily represent the official views of the various funding agencies.

REFERENCES

[1] C. B. Caldwell and M. J. Yaffe, "Development of an anthropomorphic breast phantom," *Medical Physics*, vol. 17, pp. 273-80, 1990.

[2] P. R. Bakic, M. Albert, D. Brzakovic, and A. D. A. Maidment, "Mammogram synthesis using a 3D simulation. I. Breast tissue model and image acquisition simulation," *Medical Physics*, vol. 29, pp. 2131-9, 2002.

[3] P. R. Bakic, M. Albert, D. Brzakovic, and A. D. A. Maidment, "Mammogram synthesis using a 3D simulation. II. Evaluation of synthetic mammogram texture," *Medical Physics*, vol. 29, pp. 2140-51, 2002.

[4] C. Zhang, P. R. Bakic, and A. D. A. Maidment, "Development of an anthropomorphic breast software phantom based on region growing algorithm," presented at SPIE, Medical Imaging, San Diego, CA, USA 2008.

[5] N. V. Ruiter, C. Zhang, P. R. Bakic, A.-K. Carton, J. Kuo, and A. D. A. Maidment, "Simulation of tomosynthesis images based on an anthropomorphic software breast tissue phantom," presented at Medical Imaging 2008: Visualization, Image-guided Procedures, and Modeling San Diego, CA, USA 2008.

[6] D. R. White, R. J. Martin, and R. Darlison, "Epoxy resin based tissue substitutes," *British Journal of Radiology*, vol. 50, pp. 814-821, 1977.

[7] A.-K. Carton, J. Li, M. Albert, S. Chen, and A. D. Maidment, "Quantification for contrast-enhanced digital breast tomosynthesis," presented at Medical Imaging 2006: Physics of Medical Imaging, San Diego, 2006.

[8] M. L. Hill, J. G. Mainprize, G. Mawdsley, and M. J. Yaffe, "A solid iodinated phantom material for use in tomographic x-ray imaging," *Med. Phys.*, vol. 36, pp. 4409-4420, 2009.